substitution ratios of less than 0.5 the power consumption will be substantially less than 10 W.

An example of the transmission characteristics between the input port and the thru and common drop ports is shown in Fig. 2. All channels were directed to the thru port except channels 7, 11 and 12; these were dropped to the common port. The insertion loss for the in-thru channels was 4.8–5.4 dB. The 1 and 10 dB passband widths were 0.46 and 1.43 nm for the demultiplexer and 0.53 and 1.60 nm for the multiplexer.

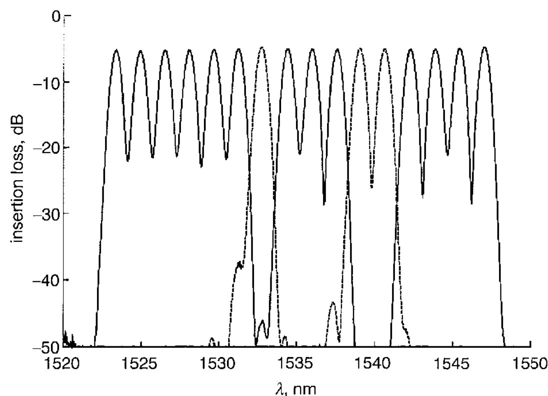

Fig. 2 *Transmission spectra from input port to thru port and to common drop port with channels 7, 11 and 12 dropped*

——— to thru port
– – – – to common drop port

We measured the isolation across a +/−15 GHz channel window, which is more than adequate for 10 Gbit/s transmission. For the thru path the isolation is limited by the demultiplexer rolloff to 41 dB. The transmissivities from the main input port to the thru port and to the common drop port, and from the common add port to the thru port, were essentially identical.

Fig. 3 shows the transmission between the input and discrete drop ports when the light is passed or blocked by the thermo-optic switches. The in-band crosstalk suppression was in excess of 46 dB. The discrete add path was similar. The input-to-discrete drop port losses were 2.6–4.0 dB and the loss between discrete add and thru ports was 2.2–3.5 dB. This minor insertion loss variation is due to an unbalanced number of waveguide intersections (0.04 dB per intersection). If necessary this could be compensated for by adding dummy crossings, without affecting other paths.

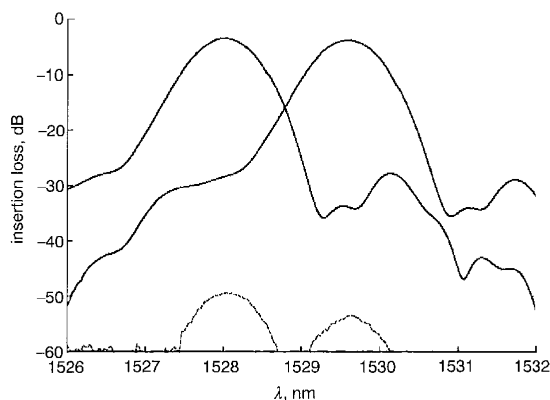

Fig. 3 *Spectra showing signal and crosstalk for in-discrete drop ports*

——— signal
– – – – crosstalk

The wavelength alignment of all the AWGs was very close, as a result of the high index uniformity films used. The peak separation of the AWGs was only 0.06 nm. We observed a maximum polarisation dependent loss at peak transmissivity between the input and thru ports of 0.2 dB.

Conclusion: We have demonstrated a low-loss, high functionality reconfigurable optical add-drop multiplexer. Thru path insertion loss is less than 6 dB with isolation in excess of 40 dB. This device forms the basis of a modular, growable, low-cost ROADM node for a long-haul or metro environment.

© IEE 2002
21 August 2002
Electronics Letters Online No: 20020901
DOI: 10.1049/el:20020901

M. P. Earnshaw and J. B. D. Soole (*Agere Systems, 600 Mountain Avenue, Murray Hill, NJ 07974, USA*)

E-mail: mpearnshaw@lucent.com

M. P. Earnshaw: Now at Lucent Technologies

References

1 OKAMOTO, K., TAKIGUCHI, T., and OHMORI, Y.: '16-channel optical add/drop multiplexer using silica-based arrayed-waveguide gratings', *Electron. Lett.*, 1995, **31**, pp. 723–724
2 SAIDA, T., KANEKO, A., GOH, T., OKUNO, M., HIMENO, A., TAKIGUCHI, K., and OKAMOTO, K.: 'Athermal silica-based optical add/drop multiplexer consisting of arrayed waveguide gratings and double gate thermo-optical switches', *Electron. Lett.*, 2000, **36**, pp. 528–529
3 VREEBURG, C.G.M., UITTERDIJK, T., OEI, Y.S., SMIT, M.K., GROEN, F.H., METAAL, E.G., DEMEESTER, P., and FRANKENA, H.J.: 'First InP-based reconfigurable integrated add-drop multiplexer', *IEEE Photonics Technol. Lett.*, 1997, **9**, pp. 188–190
4 DOERR, C.R., STULTZ, L.W., CAPPUZZO, M., LASKOWSKI, E., PAUNESCU, A., GOMEZ, L., GATES, J.V., SHUNK, S., and WHITE, A.E.: '40-wavelength add-drop filter', *IEEE Photonics Technol. Lett.*, 1999, **11**, pp. 1437–1439
5 OKAMOTO, K., OKUNO, M., HIMENO, A., and OHMORI, Y.: '16-channel optical add/drop multiplexer consisting of arrayed-waveguide gratings and double-gate switches', *Electron. Lett.*, 1996, **32**, pp. 1471–1472
6 DOERR, C.R., JOYNER, C.H., STULTZ, L.W., and MONNARD, R.: 'Wavelength-division multiplexing cross connect in InP', *IEEE Photonics Technol. Lett.*, 1998, **10**, pp. 117–119
7 GILES, C.R., BARBER, B., AKSYUK, V., RUEL, R., STULTZ, L., and BISHOP, D.: 'Reconfigurable 16-channel WDM drop module using silicon MEMs optical switches', *IEEE Photonics Technol. Lett.*, 1999, **11**, pp. 63–65

Stimulated Raman scattering in silicon waveguides

R. Claps, D. Dimitropoulos and B. Jalali

The use of the Raman effect in silicon to create optical amplification in silicon-on-insulator waveguides is investigated. The analysis shows that when using stimulated Raman scattering, it is possible to achieve up to 10 dB of signal gain in optically pumped silicon waveguides with lengths <2 cm.

Motivation and discussion: Silicon-on-insulator (SOI) has emerged as an attractive platform for planar lightwave circuits [1]. The availability of high quality SOI wafers and the complete compatibility with silicon integrated circuit (IC) technology has been the prime motivation for researchers and, more recently, for entrepreneurs. SOI devices such as arrayed waveguide gratings (AWG) and channel equalisers now compete with those realised using the silica waveguide and polymer technologies [2]. Advanced patterning and etching techniques developed and used by the IC industry can be utilised to fabricate complex periodic structures [3, 4]. The large index mismatch between the silicon core and SiO_2 lower cladding layers minimises radiation into the substrate even when extreme index modulation is performed.

Compared to the fibre technology, waveguide devices suffer from higher losses. The loss originates from both the fibre-to-waveguide coupling and propagation loss in the waveguide due to sidewall roughness, defects, and impurities. If not compensated for, this will limit the extent of on-chip integration and will, therefore, curtail the promise of integrated optics. The lack of optical gain in silicon is currently one of the major drawbacks of SOI integrated optics. The indirect bandgap prohibits the realisation silicon-based semiconductor optical amplifiers (SOAs). Further, attempts with erbium doping of

silicon have not been fruitful. However, the Raman gain coefficient in silicon is several orders of magnitude larger than that in the (amorphous) glass fibre because of the single crystal structure. In addition, the ability to confine tightly the pump signal in a small cross section lowers the threshold for stimulated Raman scattering (SRS). The gain bandwidth for the first-order Raman scattering is in excess of 100 GHz, making it possible to amplify a single WDM channel at 100 GHz spacing, or multiple channels at smaller channel spacing. Fig. 1 shows the conceptual block diagram of a generic SOI circuit making use of Raman amplifier stages to compensate for on-chip losses. The amplification can be distributed along the waveguides constituting the passive devices.

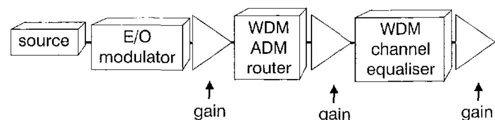

Fig. 1 *Conceptual block diagram of generic SOI circuit making use of Raman amplifier stages to compensate for on-chip losses*

Amplification can be distributed along waveguides constituting passive devices

The main feature in the spontaneous Raman spectrum of silicon corresponds to first-order Raman scattering from zone-centre optical phonons [5]. It lies at 15.6 THz with an FWHM of 105 GHz at room temperature. Other features in the spectrum correspond to two-phonon scattering and their intensity is approximately two orders of magnitude lower. This work focuses on the amplification of signals in the C-band of optical-communication networks, centred at 1540 nm, using first-order Raman scattering in silicon. The corresponding pump wavelength, of 1427 nm, is far from any absorption resonances (at 360 nm-direct transition and 1130 nm-indirect transition). From the measured first-order Raman scattering efficiency in [5], the stimulated Raman gain coefficient is calculated to be $g_s = 0.070$ cm/MW at the Stokes wavelength of $\lambda_s = 1540$ nm and the pump wavelength of $\lambda_p = 1427$ nm.

The rib SOI waveguide that is used as an example of a Raman amplifier is shown in Fig. 2. The scattering configuration selected combines a large Raman efficiency with orthogonal pump and signal polarisations. The orthogonal configuration is helpful for signal-pump isolation at the output. In addition, the wide availability of [100] SOI wafers renders this geometry favourable. The beam propagation method (BPM) simulations show (Fig. 2) that the overlap between the TE_0 (pump) and TM_0 (signal) modes in the waveguide is better than 95% across an area, A, of 2 μm^2. To account for propagation losses at the pump and signal wavelengths (γ_P and γ_S) in SOI waveguides we assume a conservative value of $\gamma_S = \gamma_P = 1$ dB/cm [6].

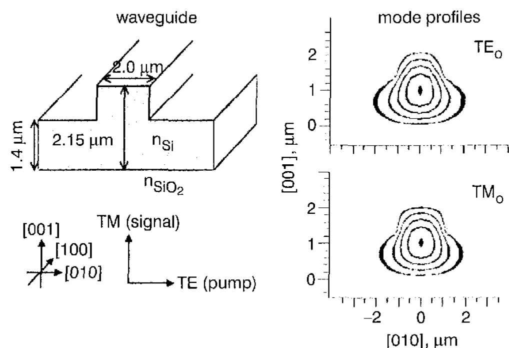

Fig. 2 *Geometry of SOI waveguide used to simulate SRS*

Orientation of waveguide is along [100] crystallographic axis in silicon

Field profiles for TE_0 and TM_0 modes are also shown demonstrating excellent modal overlap necessary for SRS

Ignoring pump depletion and assuming a negligible pump linewidth (compared to first order Stokes bandwidth) the power of the signal field at the end of the waveguide of length L, $P_S(L)$, is given as [7]

$$P_S(L) = P_S(0)\exp\left[-\gamma_R L + \frac{g_s S_P(0)}{\gamma_P}[1 - \exp[-\gamma_P L]\right] \quad (1)$$

where $S_P(0) = P_P(0)/A$, with $P_P(0)$ the input pump power. The result of (1) is shown in Fig. 3. Including the mode mismatch of 5% between signal and pump lasers along the waveguide, the results suggest that for a 1.9 cm long waveguide, a CW pump power of 475 mW (at $\lambda_P = 1427$ nm) provides an effective signal gain of 10 dB. A BPM simulation for a 2 mm long taper, coupling an 8×8 μm input waveguide to the Raman active waveguide shown in Fig. 2, shows a 0.5 dB coupling loss for the TE_0 mode.

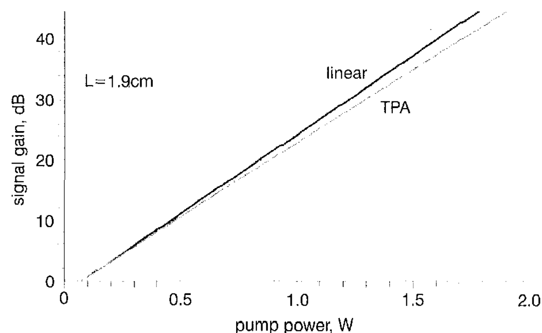

Fig. 3 *Calculated optical gain for input signal power of 1 μW*

When high field intensities propagate through the silicon waveguide, other nonlinear effects can also take place. In particular, two photon absorption (TPA) must be considered as it causes pump depletion and hence curtails SRS. As it will be shown, TPA also imposes an upper limit on the optical signal to noise ratio (OSNR) of the amplifier. Pump depletion is modelled by describing the pump propagation along the waveguide (x), in the small-γ_P limit, as:

$$P_P(x) = \frac{P_P(0)e^{-\gamma_P x}}{(1 + BxS_P(0))} \quad (2)$$

where B is the TPA coefficient for silicon at 1427 nm, $B = 3.5 \times 10^{-10}$ cm/W [8]. The result of introducing the TPA effect is included in Fig. 3. In summary, to obtain a 10 dB effective gain in the waveguide amplifier, a pump power of $P_P(0) = 500$ mW will be necessary.

The main source of noise in the signal is expected to come from amplified spontaneous Raman scattering (ASE) along the waveguide [9]. The calculated SNR, including TPA, for the device under consideration ($L = 1.9$ cm) gives a maximum OSNR of 25 dB with an input signal power of $P_S(0) = 1$ μW and a pump power of 1.0 W.

Conclusion: The prospects for a waveguide Raman amplifier using SOI technology have been analysed and quantified. The large Raman coefficient of crystalline silicon, combined with the ability to fabricate tightly confining waveguides, offers the possibility of achieving 10 dB signal gain at 1540 nm using a 1.9 cm long waveguide with 500 mW of narrowband pump power. Calculations of OSNR suggest that the main limitations originate from ASE and TPA. Brillouin [10], and Rayleigh scattering in silicon [11] are several orders of magnitude smaller than the Raman coefficient, hence their influence in OSNR is expected to be negligible.

Acknowledgments: The authors would like to thank Jia-ming Liu of UCLA for helpful discussions.

© IEE 2002
30 July 2002

Electronics Letters Online No: 20020931

DOI: 10.1049/el:20020931

R. Claps, D. Dimitropoulos and B. Jalali (*Optoelectronic Circuits and Systems Laboratory, University of California, Los Angeles, CA 90095-1594*)

E-mail: claps@ee.ucla.edu

References

1 JALALI, B., YEGNANARAYANAN, S., YOON, T., YOSHIMOTO, T., RENDINA, I., and COPPINGER, F.: 'Advances in silicon-on-insulator Optoelectronics', *IEEE J. Sel. Top. Quantum Electron.*, 1998, **4**, (6), pp. 938–947 (Special Issue on Silicon-Based Optoelectronics)

2 ROBERTS, S.W., PANDRAUD, G., LUFF, B.J., BOWDEN, C., ANNETTS, P.J., BOZEAT, R.J., FULLER, S., DRAKE, J., JACKSON, M., and ASGHARI, M.: 'NFOEC'. Denver, CO, USA, 2000, Paper 08000
3 NAYDENKOV, M., and JALALI, B.: 'Proc. SPIE'. Photonics West conference, San Jose, CA, January 2000, Vol. 3936, p. 33
4 DIAL, O., CHENG, C.C., and SCHERER, A.: 'Fabrication of high density nanostructures by electron beam lithography', *J. Vac. Sci. Technol.*, 1998, **B16**, p. 3887
5 RALSTON, J.M., and CHANG, R.K.: 'Spontaneous-Raman-scattering efficiency and stimulated scattering in silicon', *Phys. Rev. B*, 1970, **B2**, (6), p. 1858
6 SCHMIDTCHEN, J., SPLETT, A., SCHUPPERT, B., PETERMANN, K., and BURBACH, G.: 'Low loss single mode optical waveguides with large cross-section in silicon-on-insulator', *Electron. Lett.*, 1991, **27**, (16), p. 1486
7 STOLEN, R.H., and IPPEN, E.P.: 'Raman gain in glass optical waveguides', *Appl. Phys. Lett.*, 1973, **22**, (6), p. 276
8 REINTJES, J.F., and MCGRODDY, J.C.: 'Indirect two-photon transitions in Si at 1.06 μm', *Phys. Rev. Lett.*, 1973, **30**, (19), p. 901
9 AGRAWAL, G.: 'Nonlinear fiber optics' (Academic Press, London, 2001, 3rd end.)
10 GRIMSDITCH, M., and CARDONA, M.: 'Absolute cross-section for Raman scattering by phonons in silicon', *Phys. Statu. Solidi. (B)*, 1980, **102**, p. 155
11 IPPEN, E.P., and STOLEN, R.H.: 'Stimulated Brillouin scattering in optical fibers', *Appl. Phys. Lett.*, 1972, **21**, (11), p. 539

Low-threshold current GaAsSb/GaAs quantum well lasers grown by solid source molecular beam epitaxy

Po-Wei Liu, Ming-Han Lee, Hao-Hsiung Lin and Jhe-Ren Chen

Low threshold current density GaAsSb/GaAs quantum well lasers were grown on GaAs substrate using solid source molecular beam epitaxy. The laser emits 1.28 μm light output and demonstrates a very low threshold current density of 210 A/cm^2.

Introduction: 1.3 μm semiconductor lasers grown on GaAs substrates are of great interest recently because they have been recognised to be the key light sources for the optical communications in the near future. The active media used for GaAs-based 1.3 μm lasers include InGaAsN [1], quantum dots [2], and GaAsSb quantum wells (QWs) [3–5]. Among these materials, strained GaAsSb/GaAs QWs grown on GaAs substrate, which exhibit a staggered type-II band alignment, possess the potential of emitting a wavelength longer than those corresponding to the fundamental band gap energies of each constituent. The GaAsSb QW lasers reported were grown by growth methods such as metal organic vapour phase epitaxy (MOCVD) [3] and mostly by gas source molecular beam epitaxy (GSMBE) [4, 5]. Although good results have been reported for GaAsSb lasers grown by GSMBE and MOCVD, fewer good results were obtained by solid source molecular beam epitaxy (SSMBE). In this Letter, we report GaAsSb/GaAs double quantum well lasers grown by SSMBE utilising a cracked Sb monomer (Sb_1) for Sb source. The high quality of the laser is manifested by the very low threshold current density measured in the broad area devices.

Experiment: The lasers were grown on n^+GaAs (100) substrate by SSMBE. Besides the conventional Ga beam, a cracked Sb monomer and uncracked As tetramer were used in the growth of the GaAsSb. The improvement in the optical quality of the Sb-containing compound semiconductor by using Sb_1 instead of Sb_4 has been reported in [6]. The active region of the laser, which was grown at 500°C, consists of two 7 nm $GaAs_{0.66}Sb_{0.34}$ QWs embedded in GaAs barriers. Step-confined 0.1 μm $Al_{0.3}Ga_{0.7}As$ was used for the waveguide layers and 1.5 μm $Al_{0.6}Ga_{0.4}As$ was used for cladding layers. The AlGaAs layers and a 0.5 μm buffer n^+GaAs were grown at 580°C. 50 μm wide broad area lasers with different cavity lengths were fabricated by using standard photolithography, wet-etching and metallisation processes.

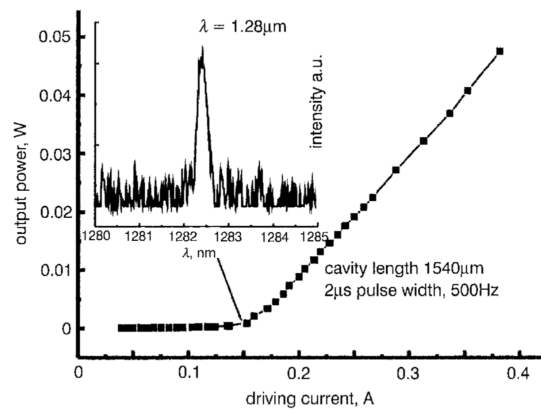

Fig. 1 *Light against current characteristic of 1.54 mm-long GaAsSb/GaAs QW laser*

Inset: *Lasing spectra of GaAsSb/GaAs QW laser*

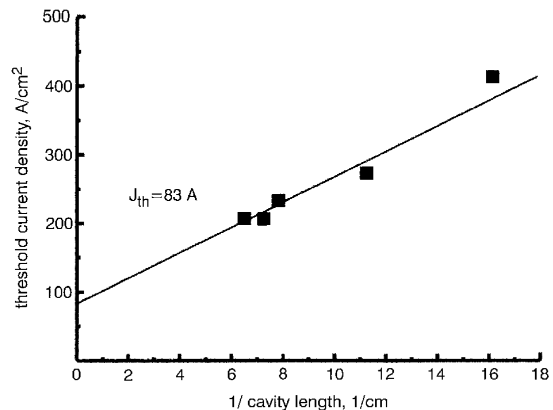

Fig. 2 *Threshold current densities against inverse cavity length*

Characteristics of laser: The fabricated lasers were tested under 2 μs pulsed mode. Fig. 1 shows the light output power against current characteristics of a 1.54 mm long laser. The threshold current and threshold current density are 162 mA and 210 A/cm^2 respectively. The result is close to the lowest values reported for GaAsSb lasers [3]. However, as can be seen in the inset of Fig. 1, our laser emits a longer wavelength at 1.28 μm in comparison to the 1.19 μm reported in [3]. In fact, the threshold current density is among the lowest values reported around the 1.3 μm region for GaAs-based QW lasers including InGaAs and InGaAsN QWs. Fig. 2 shows the cavity length dependence of the threshold current density. The threshold current density of the infinite cavity length extrapolated from the data is only 83 A/cm^2. The dependence of inverse external quantum efficiency against cavity length is shown in Fig. 3. The internal quantum efficiency is 62.8% and the internal loss fitted is 3.45 cm^{-1}. The improvement of the threshold current density is attributed to be the use of Sb_1 as the Sb source in the growth of the GaAsSb layers. The temperature characteristics of our grown laser were measured from 25 to 85°C, and the characteristic temperature is 60K, which is the typical value for GaAsSb laser reported in the literatures [3–5]. The low internal efficiency and characteristic temperature are believed to be due to the type-II structure of the GaAsSb/GaAs QW. In the type II quantum well, the spatially separated electrons and holes result in a space charge field that produces an approximately triangular electron QW in the conduction band of the GaAs barrier. As the density of the accumulated electron increases, the accordingly enhanced electric field will push the electrons toward the interface. When the electrons reach a considerable density, there will be a sufficient gain to stimulate lasing action [7]. Though the spatial separation of the electrons and holes gives a lower peak gain, it does not mean that the threshold current will be increased because the spontaneous emission is also inhibited as pointed out in [8]. However, significant blue shift of the lasing wavelength compared to the low excitation conditions will occur due